MODELING CLIMATE CHANGE IMPACTS ON COASTAL RESOURCES WITH ENHANCED SIMULATION MODEL MANTRA

KH'NG XIN YI

UNIVERSITI SAINS MALAYSIA

2021

MODELING CLIMATE CHANGE IMPACTS ON COASTAL RESOURCES WITH ENHANCED SIMULATION MODEL MANTRA

by

KH'NG XIN YI

Thesis submitted in fulfillment of the requirements
for the Degree of
Doctor of Philosophy

March 2021

ACKNOWLEDGEMENT

Completion of the PhD's program would not be possible without the assistance and support of numerous people. First and foremost, I would like to express my sincere appreciation to my supervisor, Associate Professor Dr. Teh Su Yean, for her dedicated guidance, advice, inspiration, and continuous support throughout the completion of this study. Her insightful observations and constructive criticism helped me establish the overall direction of the research and move forward with in-depth investigations. I would also like to extend my gratitude to Professor Koh Hock Lye for his constructive suggestions and concise comments on some of the research papers of the thesis. My sincere thanks also goes to my research co-supervisor, Dr. Shuhaida Shuib and Associate Professor Dr. Khairun Yahya, who provided me with a great background knowledge of biology, and who gave access to the laboratory facilities for soil salinity analysis. To all of you, thank you for spending time to read through the work and make valuable comments. Besides that, I would like to take this opportunity to thank Mr. Muhamad Naim Abd Malek for his assistance and guidance in the field and lab. I am grateful to the School of Mathematical Sciences, School of Biological Sciences, and Institute of Postgraduate Studies, Universiti Sains Malaysia for providing a safe, supportive, and stimulating working environment. Moreover, a special thanks to the administrative officers for their spirit of assistance and kindness. Financial support provided by the FRGS Grant 203/PMATHS/6711569 and partial support by RUI Grant 1001/PMATHS/8011018 is gratefully acknowledged. Last but not least, my deepest gratitude goes to my family and friends for their support, continual understanding, and encouragement throughout this study. They form the backbone and origin of my happiness when I need it the most. Thank you.

TABLE OF CONTENTS

LIST OF TABLES

LIST OF FIGURES

LIST OF SYMBOLS AND UNIT

α	water deficit response function	–
α_c	porous matrix compressibility	$m \cdot s^2 \cdot kg^{-1}$
α_h	reduction factor accounting for stress due to water deficit or salinity	–
α_L	longitudinal dispersivity	m
α_m	allometric constants for height crown	–
α_T	transversal dispersivity	m
a_{VG}	van Genuchten parameter	$m \cdot s^2 \cdot kg^{-1}$
α_1	empirical coefficient for soil water pressure head	–
α_2	empirical coefficient for soil water osmotic head	–
A_c	catchment area	m^2
A_{in}	cross-sectional area at the inflow point	m^2
$A_{m,n}$	Fourier series coefficient for the stream function	–
A_{out}	cross-sectional area at the outflow point	m^2
$A_{s,i}$	surface area of a spatial cell	m^2
b_{Ci}	leaf area per unit carbon	$m^2 \cdot g^{-1} \cdot C^{-1}$
β	inundation stress response function	–
β_c	fluid compressibility	$m \cdot s^2 \cdot kg^{-1}$
β_m	allometric constants for tree crown	–
B_{Ai}	active tissue carbon in plants	$g \cdot C \cdot m^{-2}$
$B_{Amax,i}$	maximum value attainable by B_{Ai}	$g \cdot C \cdot m^{-2}$
B_{Ci}	carbon in plant biomass	$g \cdot C \cdot m^{-2}$
B_{Ci0}	total initial biomass in a cell	$g \cdot C \cdot m^{-2}$
$B_{r,s}$	Fourier series coefficients for the concentration	–

c	integration constant	–
c_{ii}	allometric parameter	–
C	solute concentration in fluid	$kg \cdot kg^{-1}$
C^*	solute concentration of fluid source	$kg \cdot kg^{-1}$
C_{BC}	concentration of inflow at points of specified pressure	$kg \cdot kg^{-1}$
C_{CBC}	concentration of inflow at points of specified concentration	$kg \cdot kg^{-1}$
C_{in}	seawater concentration of inflowing fluid	$kg \cdot kg^{-1}$
C_m	attenuation factor used to incorporate competition with other mangroves	–
C_r	runoff coefficient	–
Cr	Courant number	–
C_{soil}	soil salinity	ppt
dh/dr	radial hydraulic gradient between the island centre and the discharge point	–
dbh	diameter-at-breast-height	cm
dbh_{max}	maximum dbh	cm
D_{ij}	dispersion tensor	$m^2 \cdot s^{-1}$
D_m	molecular diffusivity	$m^2 \cdot s^{-1}$
D_t	total water demand	m^3
ε	porosity	–
E	evaporation from the land surface	$m \cdot day^{-1}$
E_c	collection efficiency	–
E_m	inundation stress factor	–
EC_e	EC of the saturated soil-paste extract	$dS \cdot m^{-1}$
EC_w	EC of the soil-water extract	$dS \cdot m^{-1}$

E_T	reliability ratio	–
f_{Ci}	canopy dominance parameter	–
g	gravitational acceleration	$m \cdot s^{-2}$
g_{Ci}	light-use efficiency	$g \cdot C \cdot GJ^{-1}$
h	water table elevation (hydraulic head) above MSL	m
h_p	soil water pressure head	m
h_φ	soil osmotic pressure head	m
h_{p50}	soil water pressure head at which the water uptake rate is reduced by 50% during conditions of negligible salinity stress	m
$h_{\varphi 50}$	osmotic pressure head at which the water uptake rate is reduced by 50% during conditions of negligible water stress	m
h_{surge}	storm surge inundation depth	m
i	subscript for spatial step (in SUTRA) species index (in MANHAM)	–
I	identity tensor	–
I_{NF}	infiltration rate	$m \cdot day^{-1}$
j	subscript for spatial step (in SUTRA) species index (in MANHAM)	–
k	intrinsic permeability tensor	m^2
k_i	light extinction coefficient	–
k_{max}	maximum permeability	m^2
k_{min}	minimum permeability	m^2
k_r	relative permeability to fluid flow	–
K	aquifer hydraulic conductivity	$m \cdot s^{-1}$
l_{Ai}	active tissue litter loss rate	day^{-1}
l_{wi}	woody tissue litter loss rate	day^{-1}

L_{Cvi}	plant litterfall	$g \cdot C \cdot m^{-2} \cdot day^{-1}$
m	land surface slope	–
m_{Ai}	active tissue respiration rate	day^{-1}
m_{wi}	woody tissue respiration rate	day^{-1}
M_{Cvi}	plant respiration	$g \cdot C \cdot m^{-2} \cdot day^{-1}$
M_{pre}	mean precipitation rate for twelve months	$mm \cdot day^{-1}$
M_{tide}	mean tidal amplitude for twelve months	m
n	subscript for time step	–
n_d	total number of data points	–
n_p	number of plant species	–
n_{VG}	van Genuchten parameter	–
Nm	truncation order for the stream function in the x direction	–
Nn	truncation order for the stream function in the y direction	–
NN	number of nodes in the generated finite-element mesh	–
Nr	truncation orders for the salt concentration in the x direction	–
Ns	truncation orders for the salt concentration in the y direction	–
NS	number of surface cells	–
ρ	fluid density	$kg \cdot m^{-3}$
ρ_f	freshwater density	$kg \cdot m^{-3}$
ρ_s	seawater density	$kg \cdot m^{-3}$
p	fluid pressure	$kg \cdot m^{-1} \cdot s^{-2}$
p_{BC}	specified pressure boundary condition value	$kg \cdot m^{-1} \cdot s^{-2}$
p_l	parameter used for sensitivity analysis	–

$p1$	empirical coefficient	–
$p2$	empirical coefficient	–
$p3$	empirical coefficient	–
P	annual rainfall	$m \cdot yr^{-1}$
Pe	Peclet number	–
q_0	freshwater volume outflow rate per unit length of coastline	$m^2 \cdot s^{-1}$
q_b	inflows at the inland boundary	$m^2 \cdot s^{-1}$
Q_{in}	inflowing fluid source rate	$kg \cdot s^{-1}$
$Q_i(S_v)$	normalized transpiration rate as a function of the vadose zone salinity	–
$Q_{plant,i}$	total masses of plant water uptake from cell i	$kg \cdot s^{-1}$
$Q_{rain,i}$	total mass source from precipitation to cell i	$kg \cdot s^{-1}$
$Q_{t(in)}$	total inflows to the groundwater system	$m^3 \cdot s^{-1}$
$Q_{t(out)}$	total outflows from the groundwater system	$m^3 \cdot s^{-1}$
Q_p	fluid mass source	$kg \cdot m^{-3} \cdot s^{-1}$
Q_{PBC}	fluid mass source rate due to a specified pressure	$kg \cdot m^{-3} \cdot s^{-1}$
r	radial distance from the island centre	m
r_0	island radius	m
$r_{0,pre}$	pre-SLR island radius	m
$r_{0,post}$	post-SLR island radius	m
R	plant water uptake	$m \cdot day^{-1}$
R^2	coefficient of determination	–
$R_{max,i}$	maximum water uptake for species i	$m \cdot day^{-1}$
R_p	maximum potential water uptake rate	$kg \cdot m^{-3} \cdot s^{-1}$
R_{total}	total water uptake by plant	$m \cdot day^{-1}$

RWH_{req}	freshwater collection requirement for RWH	%
δ	relative difference between freshwater and seawater density	–
δ_{ij}	Kronecker delta	–
S	source/sink term accounting for precipitation, evaporation, and water extraction by plants	$kg \cdot m^{-3} \cdot s^{-1}$
S_{Ci}	leaf area of species *i*	$m^2 \cdot m^{-2}$
S_{CT}	total leaf area	$m^2 \cdot m^{-2}$
$S_{half,i}$	half-saturation constant for maximum water uptake for species *i*	$kg \cdot kg^{-1}$
SI	solar irradiance	$GJ \cdot m^{-2} \cdot day^{-1}$
S_{op}	specific pressure storativity	$m \cdot s^2 \cdot kg^{-1}$
S_{sea}	storm surge water salinity	$kg \cdot kg^{-1}$
S_m	salinity stress factor	–
S_s	source/sink term for production or loss of solute within the system	s^{-1}
S_v	vadose zone salinity	$kg \cdot kg^{-1}$
S_w	water saturation	–
S_{wres}	residual saturation	–
S_{wt}	groundwater salinity	$kg \cdot kg^{-1}$
SD_{pre}	standard deviations of precipitation rate	$mm \cdot day^{-1}$
SD_{tide}	standard deviations of tidal amplitude	m
t	time	s
μ	fluid viscosity	$kg \cdot m^{-1} \cdot s^{-1}$
U_{Cvi}	plant gross productivity	$g \cdot C \cdot m^{-2} \cdot day^{-1}$
v	fluid velocity	$m \cdot s^{-1}$
v_p	pressure-based conductance for the specified pressure source	$s \cdot m^{-2}$

v_C	concentration-based conductance for the specified solute source	$kg \cdot m^{-3} \cdot s^{-1}$
V	volume of extractable water in the freshwater lens	m^3
V_c	percentage change in lens volume	%
V_i	cell volume at node i	m^3
V_{post}	post-SLR freshwater lens volume	m^3
V_{pre}	pre-SLR freshwater lens volume	m^3
V_{RWH}	water harvesting potential	$m^3 \cdot yr^{-1}$
w_{Ci}	canopy scaling factor	–
ω_i	asymmetric weighting function at node i	–
W	net (effective) recharge rate	$m \cdot s^{-1}$
W_{post}	targeted recharge rate to maintain the pre-SLR lens volume	$m \cdot yr^{-1}$
x_T	seawater wedge toe location	m
γ_m	derived factor based on the maximum possible tree height	–
Y_t	rainwater yield	m^3
z_v	vadose zone depth	m
ζ	depth of the freshwater-seawater interface below MSL (freshwater lens thickness)	m
ζ_0	depth of aquifer base below MSL	m
ζ_{max}	maximum freshwater lens thickness	m
$\zeta_{max,pre}$	pre-SLR lens thickness	m
$\zeta_{max,post}$	post-SLR lens thickness needed to maintain the freshwater volume at the pre-SLR level	m
ζ_p	predicted lens thickness obtained from the fitted regression line	m
ξ	length to depth ratio	–
Ω	conversion factor	–

Φ	potential	m^2
θ	soil water content	$m^3 \cdot m^{-3}$
θ_s	saturated soil water content	$m^3 \cdot m^{-3}$
θ_{sp}	water content of the saturated paste	$kg \cdot kg^{-1}$
ϕ_j	symmetric bilinear or trilinear basis function at node j	–
$\Delta\rho$	density difference between freshwater and seawater	$kg \cdot m^{-3}$
Δt	time step	s
ΔV	change in water storage over a period of time	$m^3 \cdot s^{-1}$
$\Delta x, \Delta y, \Delta z$	spatial step	m

LIST OF ABBREVIATIONS

Argus ONE	Argus Open Numerical Environments
CERP	Comprehensive Everglades Restoration Plan
CMIP5	Coupled Model Intercomparison Project Phase 5
CSIRO	Commonwealth Scientific and Industrial Research Organisation
DHI	Danish Hydraulic Institute
EC	Electrical Conductivity
ENP	Everglades National Park
FDM	Finite Difference Method
FEM	Finite Element Method
FGL	Fresh Groundwater Lens
GCC	Global Climate Change
GHG	Greenhouse Gas
GIA	Glacial Isostatic Adjustment
IBM	Individual Based Model
IPCC	Intergovernmental Panel on Climate Change
IPCC AR5	IPCC's Fifth Assessment Report
IRC	International Water and Sanitation Centre
IUCN	International Union for Conservation of Nature
JMG KPP	Department of Mineral and Geoscience Kedah/Perlis/PulauPinang
JUPEM	Department of Survey and Mapping Malaysia
MANHAM	MANgrove HAMmock model
MANTRA	Coupled MANHAM and SUTRA model
MHLG	Ministry of Housing and Local Government

MIKE SHE	MIKE Système Hydrologique Européen
MMD	Malaysian Meteorological Department
MMN	Marine Monitoring Network
MODFLOW	Modular Finite-Difference Flow Model
MSL	Mean Sea Level
MT3DMS	Modular Transport, 3-Dimensional, Multi-Species model
NAHRIM	National Hydraulic Research Institute of Malaysia
NHC	National Hurricane Center
NOAA	National Oceanic and Atmospheric Administration
NRC	National Research Council
PBAPP	Perbadanan Bekalan Air Pulau Pinang
PDE	Partial Differential Equation
PIE	Plug-In Extension
PPT	Parts Per Thousand
QGIS	Quantum Geographic Information System
RWH	Rainwater harvesting
RCP	Representative Concentrated Pathway
SEAWAT	Coupled MODFLOW and MT3DMS model
SLR	Sea Level Rise
SUTRA	Saturated-Unsaturated TRAnsport
SWAP	Soil-Water-Atmosphere-Plant
SWI	Seawater Intrusion
TIF	Tagged Image File Format
UKM	Universiti Kebangsaan Malaysia
UNEP	United Nations Environment Programme

UN SDG	United Nations Sustainable Development Goal
USDA	United States Department of Agriculture
USEPA	United States Environmental Protection Agency
USGS	United States Geological Survey
USM	Universiti Sains Malaysia
WHO	World Health Organization
WMO	World Meteorological Organization
WRDA	Water Resources Development Act

PEMODELAN KESAN PERUBAHAN IKLIM TERHADAP SUMBER PESISIRAN PANTAI DENGAN MODEL SIMULASI MANTRA DIPERTINGKATKAN

ABSTRAK

Pemecutan kenaikan paras air laut dan perubahan curah hujan sebagai tindak balas terhadap perubahan iklim sedang berlaku, dan kesan ini menyarankan agar tindakan iklim (SDG 13) yang sewajarnya diambil. Peningkatan kejadian pembanjiran air laut dan pencerobohan air masin di bawah permukaan tanah akan mengurangkan jumlah ketersediaan air tawar bawah tanah akibat pemasinan air bawah tanah yang berkekalan. Tambahan pula, peningkatan tahap kemasinan tanah dan pengurangan input air tawar mampu mengubah ekosistem pesisiran pantai dengan membantu pertumbuhan tanaman yang memiliki daya toleransi kemasinan dan pembanjiran yang lebih tinggi. Fokus tesis ini adalah pemodelan dan analisis kesan perubahan iklim terhadap ketersediaan dan kualiti air bawah tanah pesisiran pantai serta potensi perubahan liputan tumbuh-tumbuhan. Untuk tujuan ini, model simulasi MANTRA dipertingkatkan dan digunakan dalam tesis ini. Model hidrologi-kemasinan-tumbuhan MANTRA dibangunkan dengan menggabungkan model persaingan tumbuhan MANHAM dan model aliran air bawah tanah dan pengangkutan zat terlarut SUTRA. SUTRA disahkan terlebih dahulu dengan ujian piawaian ketumpatan aliran untuk memastikan pemahaman dan implementasi SUTRA yang betul. Kemudian, simulasi dan analisis lebih lanjut dilakukan untuk memberikan gambaran mengenai tindak balas lensa air tawar bawah tanah di pulau atol terhadap kenaikan paras air laut dan perubahan curah hujan. Potensi penuaian air hujan untuk mengurangkan kesan kenaikan paras air laut terhadap akuifer pesisiran

pantai juga diterokai. Untuk meneliti kesan kenaikan paras air laut terhadap air bawah tanah dan tumbuhan pesisiran pantai, MANTRA dipertingkatkan untuk merangkumi fungsi tindak balas cekaman pembanjiran dan kekeringan untuk penggunaan di Pantai Acheh di Pulau Pinang. Untuk penggunaan di Coot Bay Hammock di Florida Everglades, MANTRA dipertingkatkan selanjutnya untuk merangkumi tumbuhan bersaing ketiga iaitu *buttonwood*. Tindak balas tanah lembap pesisiran pantai terhadap kenaikan paras air laut didapati amat bergantung pada topografi kawasan kajian dan ketersediaan kawasan yang sesuai untuk migrasi tumbuhan ke daratan. Hasil simulasi model menunjukkan bahawa bekalan air tawar bawah tanah tidak berdaya maju di Pulau Pinang. Tambahan pula, unjuran kenaikan paras air laut setinggi 1 m dijangka dapat mengakibatkan kehilangan liputan hutan bakau sebanyak 21% di lokasi kajian di Pantai Acheh, Pulau Pinang. Di Coot Bay, *buttonwood* dan padang rumput halofit berkemungkinan akhirnya disingkirkan, diikuti dengan penggantian takterbalikkan tumbuhan air tawar oleh komuniti bakau. Pemahaman pemodelan yang diperoleh daripada kajian ini akan berguna untuk pengurusan lestari sumber pesisiran pantai pada masa hadapan dan pembangunan daya tahan komuniti pesisiran pantai terhadap kesan perubahan iklim.

MODELING CLIMATE CHANGE IMPACTS ON COASTAL RESOURCES WITH ENHANCED SIMULATION MODEL MANTRA

ABSTRACT

Accelerated sea level rise (SLR) and precipitation change in response to climate change is well underway, the impacts of which call for appropriate climate action SDG 13. The associated increase in surface seawater inundation and subsurface saltwater intrusion will reduce the availability of fresh groundwater due to permanent salinization of groundwater. Further, increased levels of soil salinity and decreased freshwater inputs may alter coastal ecosystems by facilitating the establishment of plants with higher salinity and flooding tolerance. This thesis focuses on the modelling and analysis of climate change impacts on the availability and quality of coastal groundwater as well as on the potential changes in coastal vegetation. For this purpose, the simulation model MANTRA is enhanced and used in this thesis. The hydrology-salinity-vegetation model MANTRA was developed by coupling the vegetation competition model MANHAM and groundwater flow and solute transport model SUTRA. SUTRA is first verified against standard density-dependent flow benchmarks for the purpose of ensuring correct understanding and implementation of SUTRA. Further simulation and analysis are then performed to provide insights on the response of an atoll island's fresh groundwater lens to SLR and changes in precipitation. The potential of harvesting rainwater to mitigate the impact of SLR on coastal aquifer is also explored. To examine the impacts of sea level rise on coastal groundwater and vegetation, MANTRA is enhanced to include inundation and water stress response functions for application to Pantai Acheh of Penang. For application to Coot Bay Hammock of Florida Everglades, MANTRA is

further enhanced by incorporating a third competing vegetation. The response of coastal wetlands to SLR is found to be largely dependent on the topography of the study area and the availability of suitable areas for vegetation migration landward. Model simulation suggests that fresh groundwater is non-viable in Penang Island. Further, a projected 1-m rise in sea level is expected to result in the loss of up to 21% of mangrove coverage in the study site at Pantai Acheh of Penang Island. In Coot Bay, the buttonwoods and halophytic prairie could eventually be squeezed out, followed by irreversible landward replacement of freshwater hammocks by mangrove communities. The modelling insights from this research would be useful for future sustainable management of coastal resources and development of coastal community's resilience towards climate change impacts.

CHAPTER 1

INTRODUCTION

1.1 Global Climate Change

The Earth's climate has been undergoing unprecendented changes since the beginning of the Industrial Revolution in 1750, primarily due to anthropogenic activities. Population growth, industrial development, fossil fuel combustion, increased deforestation and land use changes, and intensified agricultural practices have greatly increased the atmospheric concentrations of greenhouse gases (GHGs) such as carbon dioxide. Continual increases in GHG concentration could intensify the natural greenhouse effect, thereby causing the Earth's surface temperature to increase. The so-called 'global warming' causes sea levels to rise, mainly due to the increased melting of the Antarctic and Greenland ice sheets, and to the thermal expansion of the oceans (Rahmstorf et al., 2007). Mean sea level rise (SLR) has accelerated to an estimated annual increase of 3.2 mm, doubling the observed rate over the last century (IPCC, 2013). However, the effect of climate change on the amount of precipitation is not globally homogeneous. An increase in water vapor of the lower troposphere induced by global warming tends to increase (decrease) the vertical upward velocity and precipitation in convection (subsidence) regions where the mean precipitation is usually high (low). This is analogous to the "rich-get-richer" mechanism proposed by previous studies (Chou and Neelin, 2004; Boucher et al., 2013), where wet places become wetter and dry places become drier.

International demand for modelling research in climate science has increased substantially since the establishment of the Intergovernmental Panel on Climate

Change (IPCC) by the World Meteorological Organization (WMO) and the United Nations Environment Programme (UNEP) in 1988. The IPCC regularly evaluates the latest technical, scientific, and socio-economic information relevant to climate change, its global and regional impacts, and adaptation and mitigation strategies. The most recent IPCC's Fifth Assessment Report (AR5) provided projections of global temperature rise and SLR by 2100 under four plausible greenhouse gas emission scenarios (Church et al., 2013; IPCC, 2014). The scenarios, known as Representative Concentrated Pathways (RCPs), include a low emissions scenario that assumes strong curtailments in GHG emissions (RCP 2.6), a high 'business-as-usual' emissions scenario that assumes continued increases in GHG emissions (RCP 8.5), and two intermediate emissions scenarios that assume continued increases in emissions until about 2050 (RCP 4.5) or 2080 (RCP 6.0), followed by emissions reductions through 2100.

As shown in Figure 1.1, global mean SLR for the late 21st century (2081-2100) is projected to be in the range of 0.26 m to 0.55 m for RCP 2.6, 0.32 m to 0.63 m for RCP 4.5, 0.33 m to 0.63 m for RCP 6.0, and 0.45 m to 0.82 m for RCP 8.5, relative to the reference period 1986-2005 (Church et al., 2013). Under the plausible worst-case RCP 8.5 scenario with the highest greenhouse gas concentrations, the IPCC has predicted a SLR of 0.52 m to 0.98 m, which is equivalent to annual rates of 8 to 16 mm. Figure 1.2 shows the projected changes in annual mean precipitation for the RCP 2.6 and RCP 8.5 scenarios. Mean precipitation is projected to increase in the equatorial Pacific Ocean, high latitudes, and mid-latitude wet regions such as Europe and North America, and to decrease in many mid-latitude subtropical dry regions

such as nothern and southern Africa. This pattern roughly matches the prediction of the "rich-get-richer" mechanism described earlier.

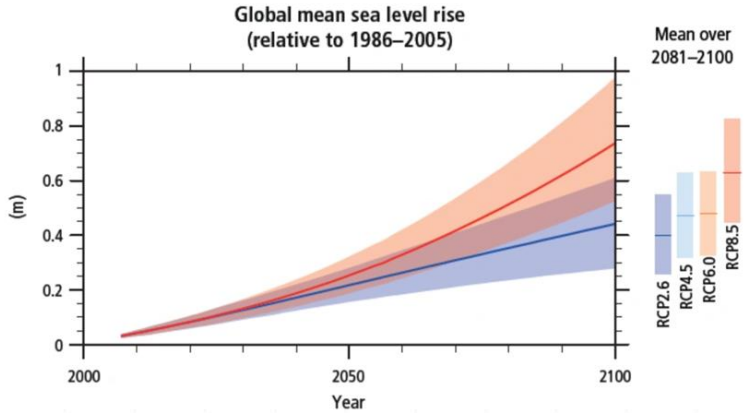

Figure 1.1: Projected global mean SLR over the 21st century relative to 1986-2005 for RCP 2.6, RCP 4.5, RCP 6.0 and RCP 8.5 scenarios (Church et al., 2013).

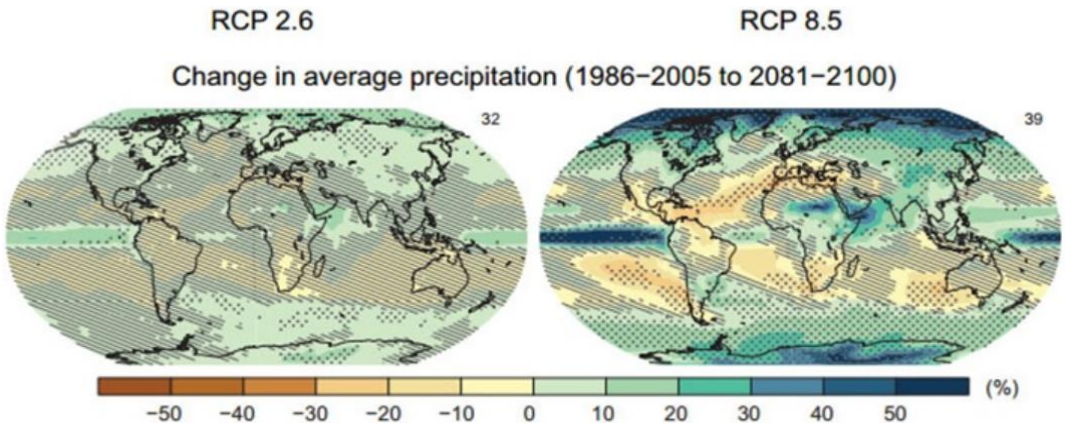

Figure 1.2: Projected change in annual mean precipitation for the late 21st century relative to 1986-2005 for RCP 2.6 and RCP 8.5 scenarios (IPCC, 2013).

1.1.1 Sea Level Rise Projections for Malaysia

The IPCC claimed that there is still a large knowledge gap in the regional assessment of climate change over Southeast Asia, primarily attributed to the limited resources for comprehensive climate downscaling exercise in the region. In Malaysia, regional climate modelling is carried out at the Malaysian Meteorological Department

(MMD), the National Hydraulic Research Institute of Malaysia (NAHRIM), the Institute of Ocean and Earth Sciences of University of Malaya (UM), and School of Environmental and Natural Resource Sciences of Universiti Kebangsaan Malaysia (UKM). Studies on SLR and its impact have been carried out by NAHRIM since 2009, and these SLR assessments are continually being updated and revised.

NAHRIM in collaboration with UKM and Commonwealth Scientific and Industrial Research Organisation (CSIRO), have developed the latest regional SLR projections for Malaysia using the Coupled Model Intercomparison Project Phase 5 (CMIP5) climate models. The models use data that represents the future contributions from the mass loss of glaciers, the surface mass balance, and the dynamic response of the Antarctic and Greenland ice sheets. The models also incorporate changes in global terrestrial water storage and Glacial Isostatic Adjustment (GIA) (Church et al., 2011; NAHRIM, 2017). Based on satellite altimetry data from 1993-2015, the observed rates of mean SLR along the coast of Malaysia are in the range between 2.8 $mm \cdot yr^{-1}$ and 4.4 $mm \cdot yr^{-1}$. As shown in Figure 1.3, the projected SLR along the coast of Peninsular Malaysia for the year 2100 is 0.67 m – 0.71 m under the RCP 8.5 scenario, with maximum value occurring in the eastern coast (Kelantan, Terengganu, Pahang, and Johor). In Eastern Malaysia, the projected SLR is 0.71 m – 0.74 m and the northern part of Sabah (Kudat) is expected to be more affected by SLR, due to its low-lying elevation.

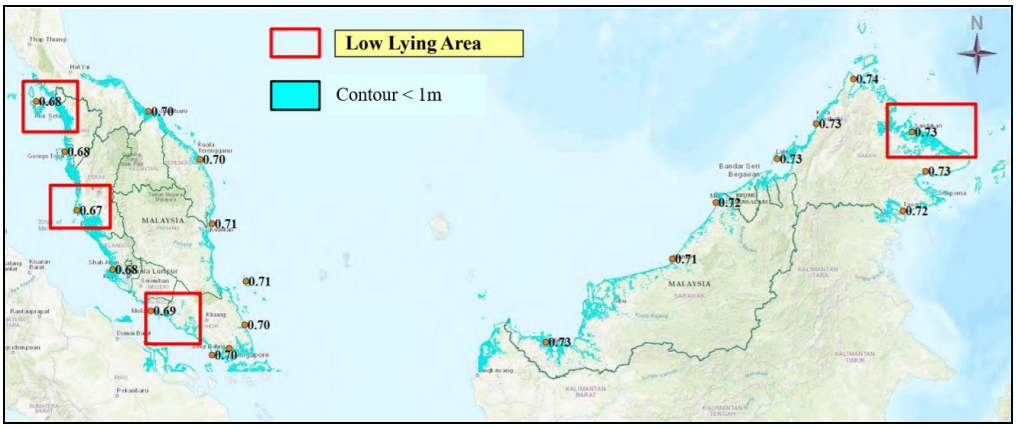

Figure 1.3: Projected SLR along the coast of Malaysia for the year 2100 under the RCP 8.5 scenario (NAHRIM, 2017).

1.2 Climate Change Impacts and Hazards

A small increase in sea level, in the order of centimetres, can significantly increase the frequency and intensity of coastal flooding events. Severe floods may result in loss of life and massive destruction to property and infrastructure. Countries and island nations with their populations and economic activities concentrated in low-lying coastal land are particularly vulnerable to SLR. This will pose a major threat to Asia-Pacific region, which is home to nearly 60% of the global population. The Solomon Islands in the western Pacific have experienced SLR rates of 7 $mm \cdot yr^{-1}$ – 10 $mm \cdot yr^{-1}$ over the past two decades, nearly three times the global average rate (Becker et al., 2012). Five vegetated reef islands have been completely lost to SLR and six more islands have suffered severe shoreline recession (Albert et al., 2016). Many coastal communities had been forced to move inland and received little or no support from local government or international climate funds. Although these unusually high SLR rates are caused by the naturally occuring El Nino event and human-induced climate change, the current conditions of Solomon Islands provide useful insights into the effects of future SLR.

A World Bank study assessed the consequences of continued SLR on 84 coastal developing countries and revealed that the impacts of SLR will be particularly severe in the following twelve countries in East Asia: China, South Korea, North Korea, Vietnam, Thailand, Philippines, Myanmar, Cambodia, Malaysia, Brunei, Indonesia, and Papua New Guinea (Dasgupta, 2018). For SLR of 1 m, 74,000 km² of coastal areas in the twelve countries are at risk of permanent inundation, and more than 37 million people will be affected. A 3-m rise in sea level would displace about 90 million people, which is equivalent to Vietnam's population, the third most populated country in Southeast Asia. In several developed countries in Asia, including Singapore and Japan, artificial islands are built in the sea for urban extension, airports, and tourist resorts. However, the rate of coastal retreat has also increased in recent decades due to rising sea levels and sinking landmasses, which requires the development of new coastal management strategies (Oppenheimer et al., 2019; Ducrotoy, 2021).

Fresh groundwater reserves in coastal areas are bounded by saline groundwater originating from the ocean (see Figure 1.4(a)). The boundary between fresh and saline groundwater is called freshwater-seawater interface. The dynamic nature of the freshwater-seawater interface is caused by a combination of factors such as change in the hydraulic gradient resulting from SLR and tidal fluctuations, precipitation variations, and excessive groundwater extraction (Bear et al., 1999; Ivkovic et al., 2012). Any decrease in groundwater recharge (e.g. SLR and reduced precipitation) leads to a decrease in the circulating freshwater flux and to a landward shift in the freshwater-seawater interface. When the mixing of seawater with freshwater beneath the land surface occurs in an area that was previously fresh, the

process is known as saltwater intrusion (Ivkovic et al., 2012). If a pumping well is located near to the migrating interface, seawater could enter the well and contaminate the water supply, as shown in Figure 1.4(b).

Dessu et al. (2018) reported that the impacts of climate change on saltwater intrusion are more significant during the dry season when there is practically less flushing flows. In the Vietnamese Mekong Delta, the saltwater intrusion zone extended 15 km inland during the wet season and up to 50 km during the dry season due to the combined effects of SLR and reduction of the Mekong River flow (Khang et al., 2008). Wickramagamage (2017) also reported that in Maldives, the freshwater lens shrinks or is completely depleted on smaller islands during the dry months from January to April. It may take up to eleven months for a freshwater lens to recover from saltwater intrusion (Terry and Falkland, 2010).

Consequently, saltwater intrusion may lead to contamination of water supplies for domestic, agricultural, and industrial use, as well as to future freshwater shortages (Wilbers et al., 2014; Li et al., 2015). The world's supply of clean freshwater has been declining steadily in recent years, prominently in Asia, North America, and South America (Gleeson et al., 2012). This will pose a significant risk in achieving the United Nations Sustainable Development Goal 6 (UN SDG6), which aims to ensure universal access to clean water and sanitation. In most poor developing countries, unclean water and poor sanitation may expose billions of people to water-borne diseases such as cholera, diarrhea, and dysentery. These diseases greatly reduce their productivity and even hasten death of those with weakened immune

systems, such as young children, the malnourished and HIV/AIDS patients (WHO, 2010).

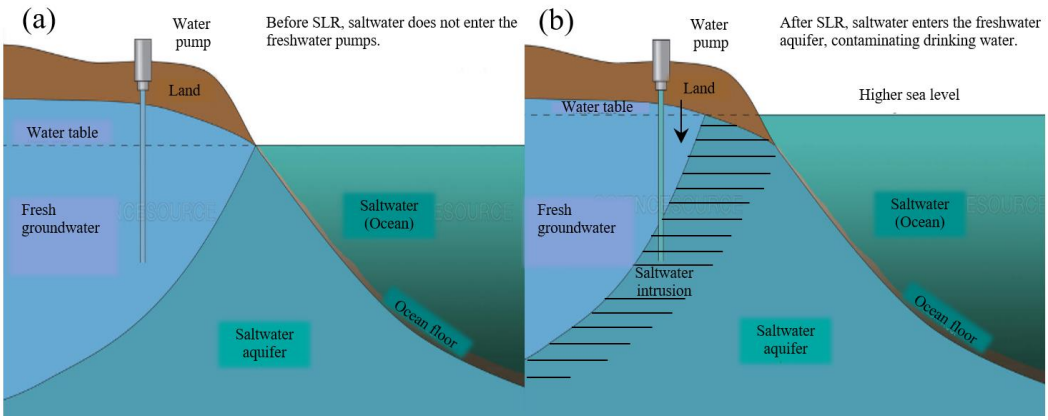

Figure 1.4: Movement of freshwater-seawater interface under (a) normal condition, and (b) in case of saltwater intrusion due to SLR.

Changes in groundwater quality can result in substantial shifts in species composition of coastal vegetation as well as the faunal communities they support, mainly through soil salinization, increased inundation frequency and depth, and through land loss due to submergence and erosion (IPCC, 2007). Plants vary greatly in their responses to salinity stress, depending on the control of ion (Na+ and Cl-) uptake by roots (Pirasteh-Anosheh et al., 2016), on the capacity to accumulate or exclude salt (Tahira et al., 2015), and on the ability to carry out the adaptive modifications such as reducing the transpiration rate (Iyengar and Reddy, 1996). In salinity-tolerant species (e.g. mangroves and saltwater marshes), these main physiological mechanisms can function effectively even at high salinity levels, whereas in salinity-intolerant species (e.g. hardwood hammocks and freshwater marshes), the mechanisms may break down. Excess salts in plants can reach toxic levels, which causes premature leaf senescence, reduction in photosynthetic capability, and ultimately leads to retarded plant growth and development (Munns, 2002). The germination of seven freshwater

marsh species of the central Gulf of Mexico were negatively affected by saltwater intrusion and soil salinization due to SLR (Sánchez-García et al., 2017). Increased salintiy would result in landward encroachment of salinity-tolerant wetland communities, as reported in the previous literature (Perry and Hershner, 1999; Sutter et al., 2014). In South Florida, the rate of inland migration of the coastal mangrove-marsh ecotone has accelerated substantially in the past century, which is probably attributed to the accelerated SLR (3 $mm \cdot yr^{-1}$ – 4 $mm \cdot yr^{-1}$) along with reduction in natural freshwater flows through the Everglades (Wanless et al., 1994; Ross et al., 2000, Krauss et al., 2011; Smith et al., 2013).

Additional habitat losses are likely to occur as a result of landward migration being constrained by topography, coastal development, or shoreline stabilization structures (Small and Nicholls, 2003; Fish et al., 2008). The combined effects of these natural and anthropogenic disturbances could potentially threaten the wetlands' ability to continually provide ecosystem services. Furthermore, SLR and precipitation changes will have impact on the productivity and yield of many agricultural crops such as rice, notably in Bangladesh, because they are highly sensitive to excessive concentration of salt (Letey and Dinar, 1986; Chinnusamy et al., 2005). About 30% of the world's paddy fields are affected by excess salinity (Rowell, 1994). This may undermine UN SDG2 that aims to end hunger, achieve food security and improved nutrition, and promote sustainable agriculture. Saltwater intrusion has also resulted in conversion of agricultural lands to brackish or saline aquaculture (e.g. shrimp or rice-shrimp systems) in many low-lying coastal areas of South and Southeast Asia (Dang, 2019).

1.3 Problem Statement

In the near future, climate change will have serious implications for fresh groundwater availability and agricultural productivity through alterations in hydrological and salinity regimes. It is doubtful whether all affected nations can meet the goals of UN SDG2 and SDG6. This necessitates the formulation of sustainable coastal management through proper assessment and utilization of the available resources. Commonly, groundwater monitoring approaches often rely on manual or automated measurements of groundwater level in boreholes (Cherry and Clarke, 2008). However, borehole monitoring networks provide sparsely distributed point information, which can be insufficient to understand the groundwater flow system in complex geological settings (Lee and Jones-Lee, 2000). Furthermore, there exist temporal lags in the vegetation responses to groundwater level fluctuations (Chui et al., 2011). Hence, dense field observation data spanning many decades or years are required to assess the complete responses of groundwater and vegetation to climate change, but these are often lacking. To understand the potential implications of sea level and climatic variability on coastal resources, it is necessary to develop a coupled model for simulating the groundwater flow and vegetation growth dynamics.

Recent attention has been given to the possibility of injecting water into aquifers to enhance groundwater recharge or to establish hydraulic barriers against saline intrusion (Pool and Carrera, 2010). Rainwater harvesting (RWH) has emerged as a viable alternative freshwater source of groundwater recharge that utilize rainwater and its runoff (Post et al., 2018; Saleem et al., 2018), compared to the expensive desalination and water recycling technologies. Generally, it aims at controlling saltwater intrusion, improving water quality, raising groundwater levels, reducing

flood flows, relieving over-pumping, and possibly preserving native plant communities (Todd, 1974). The great potential of this approach in repulsion of intruded saline wedge has been suggested by a number of researches (Mahesha and Nagaraja, 1996; Vandenbohede et al., 2009; Javadi et al., 2015). However, the role of RWH in alleviating the loss of groundwater aquifers due to climate change impacts, has not yet been adequately quantified. There is currently no official quantitative guidance on RWH as an artificial recharge technique to sustainably restore groundwater aquifers.

1.4 Purpose and Significance of the Study

This thesis focuses on modelling the impacts of climate change on groundwater and coastal vegetation, with assistance of a coupled hydrology-salinity-vegetation model MANTRA. Inputs to MANTRA include tide, precipitation, topography, geology, and vegetation data. Two study sites, one in Penang and another in Florida Everglades, where some data on hydrology and vegetation dynamics relevant to the simulation are readily available, are chosen for this study. Scientific monitoring and assessment provide basic characterization of the coastal resources of an area, improve the understanding of the distribution, extent, and pathways of saltwater intrusion, and yield quantitative information on vulnerability and risks of coastal resources to climate change. The modelling insights from this study is vital for sustainable management of coastal resources and development of coastal community's resilience towards climate change impacts. The conjunctive use of rainwater and groundwater resources is explored to provide sufficient water supply for the potential future water scarcity caused by climate change. The assessment of coastal vulnerability to climate-related impacts via MANTRA simulations can further reshape regulatory

decisions on the coastal development. Local governments could impose restrictions that limit development densities in identified vulnerable areas and encourage conservation of undeveloped coastal uplands to accommodate the landward migration of wetlands (Jessica, 2011). This modelling analysis can be applied to other coastal regions when data are available.

1.5 Research Questions

More specifically, the following research questions will be addressed:

1. Can a coupled hydrology-salinity-vegetation model improve our understanding of the current and future potential impacts of climate change on the coastal environment?
2. What are the main geo-hydrologic parameters that will affect fresh groundwater availability in coastal aquifers?
3. How does climate change threaten food security (SDG2), water security (SDG6), and ecosystem services?
4. How much RWH capacity is needed to mitigate the loss of groundwater aquifer due to SLR?
5. How accurate are the simulation results from the model developed for the study sites?

1.6 Objectives of Thesis

The objectives of this thesis are as follows:

1. To analyze the feasibility of increasing groundwater recharge through rainwater harvesting for mitigating the effect of salinity intrusion induced by SLR.
2. To revise the vegetation module in the coupled hydrology-salinity-vegetation model MANTRA for more robust simulations of climate change impacts on coastal groundwater and vegetation in two (2D) and three spatial dimensions (3D).
3. To examine the impacts of sea level rise on groundwater and vegetation at Pantai Acheh of Penang and Coot Bay Hammock of Florida Everglades.

1.7 Scope and Organization of Thesis

This thesis begins in Chapter 1 with an introduction to climate change and its impacts on groundwater and coastal vegetation, drawing insights from the experience of the climate change that occurred in the past. This is followed by the problem statement, purpose and significance, research questions, and objectives of the study. The chapter concludes with the scope and organization of this thesis.

Chapter 2 provides a review of related literature, beginning with an introduction to saltwater intrusion modeling. Simplified conceptual model of groundwater flow system is introduced to enable the development of analytical solutions for saltwater intrusion phenomena in coastal aquifers. Their capabilities and shortcomings are discussed. This is followed by a brief exploration of numerical models and their merits. Benchmark examples are provided to determine the accuracy and reliability

of numerical groundwater flow models. This chapter also provides discussion on the modeling of reduction of plant water uptake due to water, salinity, and inundation stress. The aim is to motivate the development of an enhanced coupled hydrology-salinity-vegetation model MANTRA in this thesis. Artificial groundwater recharge through RWH is presented, along with several techniques used to estimate the optimum storage tank size.

In Chapter 3, the groundwater model SUTRA is discussed and verified against two standard density-dependent flow benchmarks, namely the Henry saltwater intrusion problem and the Elder salt convection problem. An analytical formula is derived for the thickness and volume of the freshwater lens. Sensitivity analysis is performed to identify the main geo-hydrologic parameters affecting freshwater lens thickness in island aquifers. Numerical simulations are carried out using SUTRA to further explore the relation between the identified parameters and freshwater lens thickness. Model validation is performed by comparing the simulation results with the analytical solutions for lens thickness. The validated SUTRA model is used to estimate the extent of salinization and the availability of freshwater resources under the combined impact of SLR and precipitation change. The last section provides an estimate of the RWH capacity needed to mitigate the loss of groundwater aquifer due to SLR, with the recommended storage tank size.

The modelling of the feedback interactions between groundwater and vegetation will be discussed in Chapter 4. This leads to MANTRA, a model developed in this thesis by linking the groundwater model SUTRA and the existing USGS's two-species vegetation competition model MANHAM. An overview of the dynamic coupling

between SUTRA and MANHAM is provided. Some enhancements are made to the MANHAM module in MANTRA to establish a more realistic representation of groundwater-vegetation interactions for this research. The enhanced MANTRA is used to simulate the impact of SLR on the sustainability of groundwater and mangrove succession and zonation at Pantai Acheh, Penang Island. Field measurements and laboratory analysis of soil salinity are carried out for model verification purposes. Implications for food (SDG2) and water (SDG6) security in Penang Island are discussed and the fragile state of Penang's water resources is highlighted. Some measures are recommended to ensure sustainable water resources utilization in Penang for achieving food and water security.

SLR threatens low-lying coastal ecosystems in southern Florida. In Chapter 5, the enhanced MANTRA is applied to the succession of forests covered with hardwood hammocks, buttonwoods, and mangroves in Coot Bay Hammock of Florida Everglades. An attempt is made to verify a past research study for model verification purpose. MANTRA is enhanced to include buttonwood as the third competing species with the aim to provide a more realistic evaluation of the coastal landscape transformation under future SLR scenarios. We relate the results of Coot Bay Hammock case study to the ecological impacts in southern Florida. Some future research needs are also recommended for adaptation in management practices that will maximize ecological resilience in southern Florida. Chapter 6 presents a summary of findings, conclusions, and recommendations for further research.

CHAPTER 2

LITERATURE REVIEW

2.1 Introductory Chapter

This chapter begins with an introduction to saltwater intrusion modeling, followed by a review of analytical and numerical models for saltwater intrusion phenomena in coastal aquifers. This chapter also provides discussion on the modeling of reduction of plant water uptake due to water, salinity, and inundation stress that motivates the development of an enhanced coupled hydrology-salinity-vegetation model MANTRA. Lastly, the sustainability of using rainwater harvesting (RWH) as artificial recharge to counteract the loss of groundwater aquifer due to SLR, along with several techniques used to estimate the optimum storage tank size is discussed.

2.2 Introduction to Saltwater Intrusion Modeling

Spatial and temporal dynamics of groundwater level and salinity are primarily determined by the groundwater recharge and discharge conditions, by the distribution of groundwater flow, and by the structure of the groundwater system (Yu and Wang, 2012). The rates of change in groundwater level and salinity are relatively slow under natural conditions. However, the acceleration in SLR and changes in precipitation driven by climate change may intensify the variations in groundwater level and salinity, resulting from the imbalance between groundwater recharge and discharge. A switch in water balance from positive to negative may cause the intrusion of saline water into freshwater aquifers, potentially resulting in groundwater quality degradation. It could take significant time and cost to restore contaminated groundwater aquifers.

Effective management plans on coastal saltwater intrusion problems are essential to protect the quality of water resources against contamination. This leads to the development and improvement of groundwater models, which consist of a set of mathematical equations to simulate the movement of groundwater and contaminants (salts) in the subsurface environment. A complete reconstruction of the field system is not feasible, mainly because there is rarely sufficient data to completely describe the system in comprehensive details. Therefore, effective groundwater models are based on certain simplifying assumptions (e.g. aquifer heterogeneity or anisotropy, flow direction, chemical reactions) that reduce complexity while retaining sufficient detail and resolution to adequately represent the hydrological behaviour of groundwater systems.

Modeling of saltwater intrusion has been extensively studied through the sharp-interface models and dispersive-interface (density-dependent) models. The sharp-interface approach was first introduced by Badon Ghyben (1889) and Herzberg (1901), assuming that freshwater and seawater are immiscible and are separated by an abrupt interface. Glover (1959), Strack (1976), and Montoglou (2003) have used the Badon Ghyben-Herzberg approximation to develop analytical models for predicting the location of the salt wedge in groundwater flow system. This approach is widely used for the preliminary assessment of the hydrogeological system due to its computational simplicity and less intense data requirements. More sophisticated methods have also been used to incorporate climate change factors, such as rise in sea level, within a simplified sharp-interface modeling framework (Henry, 1959; Werner and Simmons, 2009).

The dispersive-interface approach accounts for the presence of salinity transition zone between freshwater and seawater. The dynamic behaviour of transition zone is controlled by the hydrogeological characteristics of the aquifer, tidal flux, and seasonal changes in groundwater recharge (Cooper, 1959; Ataie-Ashtiani et al., 1999). Henry (1964) presented a semi-analytical solution for saltwater intrusion under steady-state conditions considering the effects of dispersion. The first numerical solution of the Henry problem was provided by Pinder and Cooper (1970) for transient conditions. They solved the flow equation using an alternating-direction, implicit finite-difference scheme, and the salt transport equation was solved with the method of characteristics. Lee and Cheng (1974) formulated a finite element model using stream functions to obtain a steady-state solution for the convective-dispersive transport equation. The numerical results showed good agreement with the results of Henry (1964) and field data obtained by Kohout (1964) in the Biscayne aquifer, Florida. Segol et al. (1975) and Segol and Pinder (1976) used the Galerkin finite element technique to solve the transport equation with a velocity-dependent dispersion coefficient.

Many dispersive-interface numerical models have been formulated in public domain as well as on commercial basis, together with the continual advances made in computing power and numerical techniques. Among the most notable sources for such codes are government agencies, such as SWAT from the U.S. Department of Agriculture (USDA) laboratories, MODFLOW and SUTRA from the U.S. Geological Survey (USGS), FEMWATER from the U.S. Environmental Protection Agency (USEPA), and ParFLOW and TOUGH2 from the Lawrence Berkeley National Laboratory. These simulation models serve as a valuable decision-making

tool to develop better understanding of saltwater intrusion mechanism, to anticipate future data requirements, to provide more reliable estimates of water budgets, to forecast the consequences of future management actions on the groundwater regime, and to explore viable alternative management strategies (Moran, 2016).

2.3 Analytical Solutions for Saltwater Intrusion

Ghyben-Herzberg Solution

Analytical solution can be obtained based on the assumption that the groundwater flow system is in dynamic equilibrium between steady freshwater flow and static seawater, separated by a sharp interface. The Dupuit-Forchheimer approximation is adopted where the flow is predominantly horizontal, the vertical resistance to flow is neglected, and the pressure distribution is hydrostatic (Dupuit, 1863; Forchheimer, 1886). As shown in Figure 2.1, the thickness of the freshwater zone can be computed using the Ghyben-Herzberg formula (Badon Ghyben, 1889; Herzberg, 1901; Post, 2018):

$$\zeta = \frac{\rho_f}{\rho_s - \rho_f} h = \frac{1}{\delta} h, \tag{2.1}$$

where ρ_f and ρ_s (kg·m^{-3}) are the freshwater and seawater densities respectively, δ (dimensionless) is the relative difference between freshwater and seawater density, h (m) is the water table elevation (hydraulic head) above mean sea level (MSL), and ζ (m) is the depth of the freshwater-seawater interface below MSL.

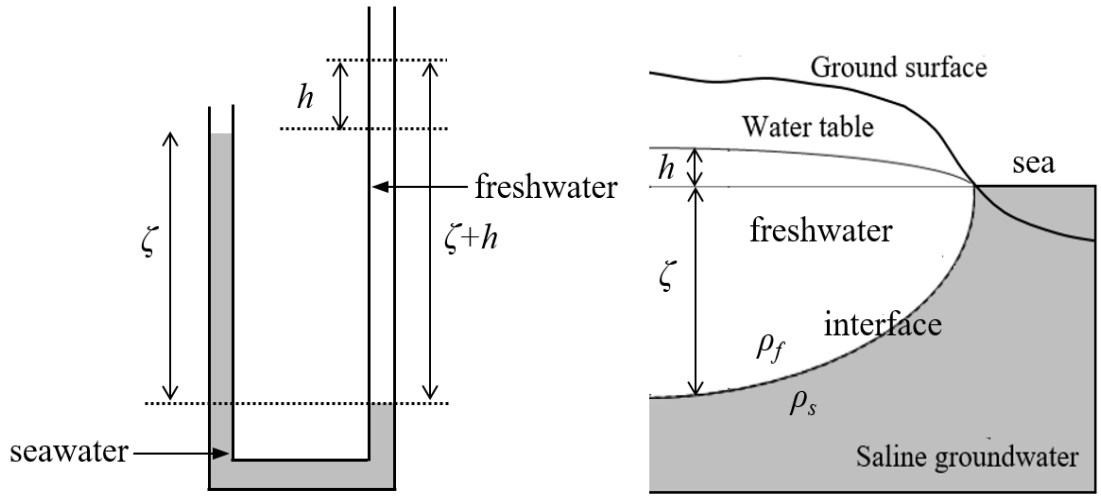

Figure 2.1: The Badon Ghyben-Herzberg principle: a freshwater-seawater interface in an unconfined coastal aquifer.

The average densities of freshwater and seawater are 1000 kg·m^{-3} and 1025 kg·m^{-3}, respectively, and thus ζ is approximately equal to 40h and is always positive. This implies that a fall of the water table by 1 m will eventually lead to a rise of the freshwater-seawater interface by 40 m. In the case of phreatic aquifers, the Dupuit-Forchheimer approximation cannot account for the seepage face that may develop above MSL, as illustrated in Figure 2.2 (Houben, 2015). The entire seepage area potentially constitutes a vertical flow feature since the seepage boundary condition allows discharge to take place, and thus the Dupuit assumption may predict a lower water table in the vicinity of pumped wells.

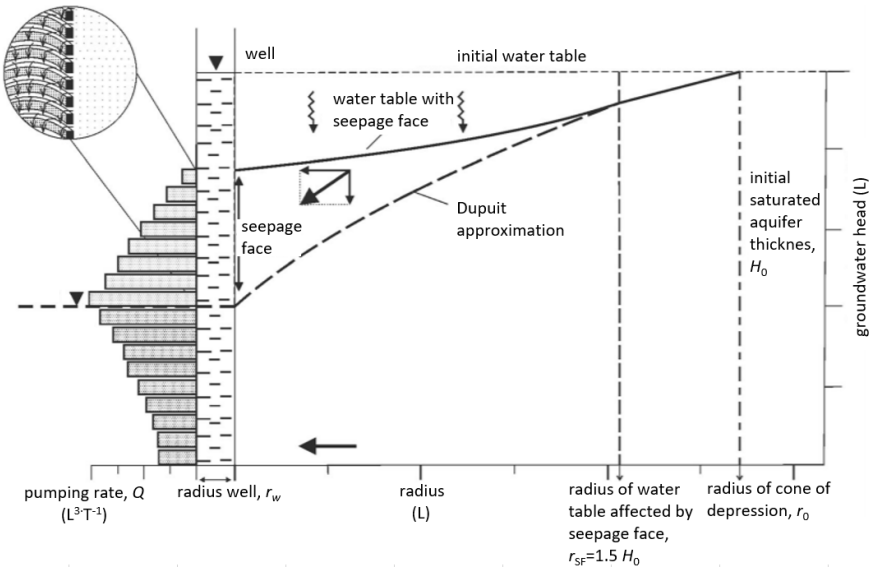

Figure 2.2: Schematic sketch of a seepage face in a well screened in an unconfined aquifer (Houben, 2015).

Strack (1976) Analytical Solution

Exact solutions for sharp-interface flow, in which the freshwater and seawater are immiscible and separated by a sharp interface, can be obtained with the Strack's potential (Strack, 1976; Koussis et al., 2012). Conceptualization of simplified aquifer settings is shown in Figure 2.3. The toe of seawater wedge, x_T (m) represents a point where the freshwater-seawater interface intersects the aquifer basement and comprises a typical measure of the extent of saltwater intrusion. The aquifer domain is separated into two zones, with freshwater flow in Zone 1 (inland of the interface, $x \geq x_T$) and interface flow in Zone 2 (bounded by the ocean boundary at $x = 0$ and the toe location x_T). In the analytical solution of Strack (1976), the Dupuit-Forchheimer assumption is applied to the freshwater flow, and the Ghyben-Herzberg relation is utilized to define the interface depth. The freshwater head is constant along the vertical in the freshwater zone and is a function of horizontal coordinates only, $h_f = h_f(x, y)$, whereas flux is neglected in the saltwater zone. Using the discharge potential

method of Strack (1976), the potential functions for Zone 1 and Zone 2 for the aquifer are defined as:

$$\text{Zone 1}: \Phi = \frac{1}{2}\left[\left(h+\zeta_0\right)^2 - \left(1+\delta\right)\zeta_0{}^2\right], \tag{2.2}$$

$$\text{Zone 2}: \Phi = \frac{1+\delta}{2\delta}\left[\left(h+\zeta_0\right) - \zeta_0\right]^2. \tag{2.3}$$

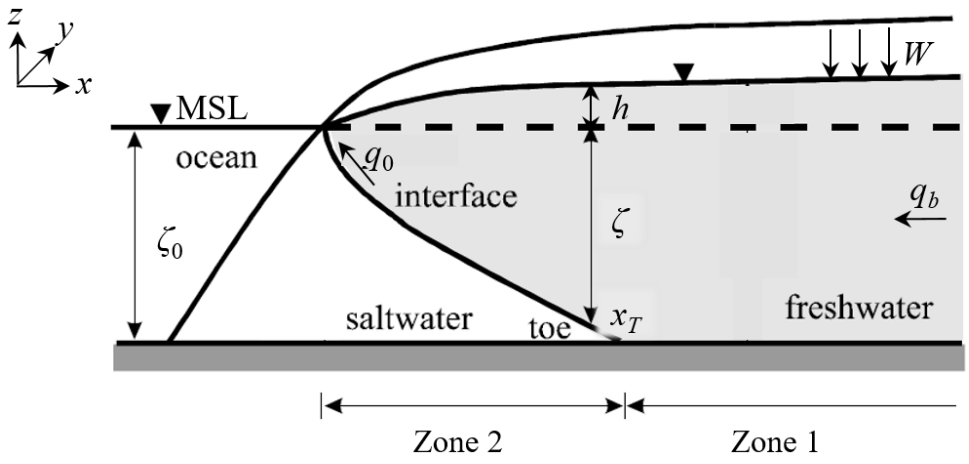

Figure 2.3: Conceptualization of a steady-state sharp interface for unconfined aquifer setting (Morgan et al., 2014).

Here, Φ (m^2) is the potential and ζ_0 (m) is the depth of aquifer base below MSL. These potential functions and their first derivatives are continuous across the multiple zones of the aquifer and satisfy the Laplace equation in two horizontal spatial dimensions, $\nabla^2\Phi = 0$, in the *x*-*y* plane (Felisa et al., 2013). Consider a vertical cross-section of an unconfined aquifer with net recharge rate, W ($m \cdot s^{-1}$), where y is fixed, the governing equation is (Cheng and Ouazar, 1999):

$$\frac{d^2\Phi}{dx^2} = -\frac{W}{K}, \quad D = \{x : x \geq 0\} \tag{2.4}$$

where K ($m \cdot s^{-1}$) is the aquifer hydraulic conductivity. Boundary conditions are:

$$\Phi = 0 \text{ at } x = 0, \text{ and } \frac{d\Phi}{dx} = \frac{q_0}{K} \text{ at } x = 0, \tag{2.5}$$

where q_0 ($m^2 \cdot s^{-1}$) is the freshwater volume outflow rate per unit length of coastline. The solution of Equation (2.4) subject to Equation (2.5) is

$$\Phi = -\frac{W}{2K}x^2 + \frac{q_0}{K}x. \quad D = \{x : x \geq 0\} \tag{2.6}$$

By substituting the potential value defined in Equation (2.6) into Equations (2.2) and (2.3), the hydraulic head, h (m) can be computed depending on the zone:

$$\text{Zone 1}: h = \sqrt{\frac{2q_0x - Wx^2}{K} + (1+\delta)\zeta_0^2} - \zeta_0, \quad D = \{x : x \geq 0\} \tag{2.7}$$

$$\text{Zone 2}: h = \sqrt{\left(\frac{\delta}{1+\delta}\right)\frac{2q_0x - Wx^2}{K}}\ . \quad D = \{x : x \geq 0\} \tag{2.8}$$

The depth of the interface (ζ) can be deduced from the hydraulic head using the Ghyben-Herzberg relation (2.1). The location of the wedge toe (x_T) is obtained through substituting $h = \delta \cdot \zeta_0$ in Equations (2.7) and (2.8) (Cheng and Ouazar, 1999). In situations where inflows from rainfall exceed the combined outflows from evapotranspiration and pumping, the net recharge rate is positive ($W > 0$). In saltwater intrusion cases, W value of either negative (total inflow < total outflow) or

zero (total inflow = total outflow) is considered. Therefore, the location of wedge toe, x_T is

$$x_T = \begin{cases} \dfrac{q_0}{W} - \sqrt{\left(\dfrac{q_0}{W}\right)^2 - \dfrac{K\delta\left(1+\delta\right)\zeta_0^2}{W}} & \text{if } W < 0, \\ \dfrac{K\delta\left(1+\delta\right)\zeta_0^2}{2q_0} & \text{if } W = 0. \end{cases} \tag{2.9}$$

Saltwater Intrusion Vulnerability Indicators

Various saltwater intrusion assessment methods have been developed based on the Strack (1976) analytical solution (Pool and Correra, 2011; Werner et al., 2012). Werner et al. (2012) used the equations of Strack (1976) as the basis for developing rapid assessment of saltwater intrusion vulnerability resulting from changes in sea level, net recharge (W), and inflows at the inland boundary (q_b). The representative indicator of saltwater intrusion extent is the rate of change in the saltwater wedge toe location in respond to changes in system stresses, as presented in Table 2.1. Werner and Simmons (2009) reported that the impact of SLR in unconfined coastal aquifers is smaller in flux-controlled systems (where groundwater discharge to the sea remains constant) than in head-controlled systems (where groundwater hydraulic head remains constant at the inland boundary). Flux control can be achieved by adjusting the upstream groundwater management whereas head control can be achieved through connection to a regulated surface water body, ensuring a certain stage at that boundary.

Table 2.1: Saltwater intrusion vulnerability indicator equations (Werner et al., 2012).

	Flux-controlled setting	Head-controlled setting
SLR	$\frac{\partial x_T}{\partial \zeta_0} = \frac{q_0 M}{\zeta_0 W \sqrt{1-M}}$ (2.10)	$\frac{\partial x_T}{\partial \zeta_0} = \frac{q_0 M}{\zeta_0 W \sqrt{1-M}} + \frac{q_0 M}{\delta \zeta_0 W}\left(\frac{1-\sqrt{1-M}}{\sqrt{1-M}}\right)$ (2.11)
Change in W	$\frac{\partial x_T}{\partial W} = \frac{q_0 M}{2W^2 \sqrt{1-M}}$ (2.12)	$\frac{\partial x_T}{\partial W} = \frac{q_0 M}{2W^2 \sqrt{1-M}} + \frac{q_0}{2W^2}\left(\frac{1-\sqrt{1-M}}{\sqrt{1-M}}\right)$ (2.13)
Change in q_b	$\frac{\partial x_T}{\partial q_b} = \frac{1}{W}\left(1-\frac{1}{\sqrt{1-M}}\right)$,	$M = \frac{K\delta(1+\delta)\zeta_0^2}{\left(q_0^2/W\right)}$. (2.14)

2.3.1 Shortcomings in Analytical Solutions

Sharp-interface analytical models work reasonably well for most large islands and coastal groundwater systems that have a relatively thin transition zone compared with the thickness of freshwater lens. However, atoll islands generally have thin freshwater lens overlying a much thicker transition zone, which cannot be realistically represented by a sharp-interface model (Lu et al., 2013). Such approximation may overestimate the extent of saltwater intrusion (Pool and Carrera, 2011), and thus underestimate the maximum allowable pumping rate. Several attempts have been made to realistically model the dispersive interface by taking into account the mixing of freshwater and seawater (Paster and Dagan, 2008). Henry (1964) developed a steady-state semi-analytical solution for saltwater encroachment in a confined coastal aquifer, including the effect of dispersion. The Henry's solution has been used for benchmarking density-dependent flow models, but it has limited usefulness in simulating saltwater intrusion in real aquifers as only diffusion and no dispersion is simulated. Alternative solutions to the Henry problem were published later by Segol (1994), Simpson and Clement (2004), and Zidane (2012). Although the analytical models of density-dependent flow are more realistic than sharp-